International Journal of Microwave and Wireless Technologies

cambridge.org/mrf

Design and analysis of a compact microstrip lowpass–bandpass diplexer with good performance for wireless applications

Abbas Rezaei[1], Salah I. Yahya[2,3] and Leila Nouri[4,5]

[1]Department of Electrical Engineering, Kermanshah University of Technology, Kermanshah, Iran; [2]Department of Communication and Computer Engineering, Cihan University-Erbil, Erbil, Iraq; [3]Department of Software Engineering, Faculty of Engineering, Koya University, Koya KOY45, Iraq; [4]Institute of Research and Development, Duy Tan University, Da Nang 550000, Vietnam and [5]Faculty of Electrical – Electronic Engineering, Duy Tan University, Da Nang 550000, Vietnam

Research Paper

Cite this article: Rezaei A, Yahya SI, Nouri L (2023). Design and analysis of a compact microstrip lowpass–bandpass diplexer with good performance for wireless applications. *International Journal of Microwave and Wireless Technologies* **15**, 1099–1107. https://doi.org/10.1017/S1759078722001465

Received: 26 September 2022
Revised: 30 November 2022
Accepted: 2 December 2022

Keywords:
Group delay; insertion loss; lowpass–bandpass; microstrip diplexer; wireless

Author for correspondence:
Leila Nouri, E-mail: leilanouri@duytan.edu.vn

Abstract

This paper presents the design of a novel lowpass–bandpass diplexer with compact size and good performance using microstrip cells. For this purpose, two microstrip lowpass and bandpass filters are separately designed and mathematically analyzed. The proposed microstrip diplexer has a novel and simple structure. It occupies a compact area of 0.037 λg^2 (722 mm^2), and its insertion loss and S_{11} at both channels are low. The insertion loss at the lower and upper channels is only 0.047 and 0.16 dB, respectively. Meanwhile, both channels are flat with the maximum group delay of 1.68 ns which is the lowest compared to the previously reported diplexers mentioned in this paper. To design the proposed diplexer, first, a lowpass diplexer with good performance is designed which has low losses and a good figure of merit. It has a flat passband with a sharp roll-off. Then, to achieve the proposed diplexer, a bandpass resonator is added to the lowpass filter without any extra matching circuit, which saves the overall size. The proposed diplexer is designed, simulated, and fabricated, where the simulation and measurement results are close.

Introduction

A common communication channel can be shared with two different devices using a diplexer. A lowpass–bandpass diplexer shares a common antenna between two distinct lowpass and bandpass signals. According to the cut-off frequency of the lowpass channel and the resonance frequency of the bandpass channel, it can be used for different wireless applications. The design of a lowpass–bandpass diplexer is much more complicated than the filters and bandpass–bandpass diplexers, because we have to design two different filters and connect them with a high isolation between the lowpass and bandpass channels. Designing compact diplexers with good performance is important for the wireless networks industry. Several types of lowpass–bandpass diplexers [1–8] and bandpass–bandpass diplexers [9–15] have been reported. Designing lowpass–bandpass diplexers is less common than the bandpass–bandpass diplexers. The bandpass–bandpass diplexers need only one resonator to create two bandpass filters (BPFs), whereas the lowpass–bandpass diplexers need to design two different resonators, i.e. lowpass and bandpass. A dual-mode bandpass resonator with an elliptic function lowpass resonator is combined to obtain a lowpass–bandpass diplexer in [1]. This diplexer has several disadvantages, such as large size, a narrow bandpass channel, high insertion loss, and high common port S_{11} at both channels. Similarly, the lowpass–bandpass diplexer presented in [2] occupies a large area with a narrow bandpass channel and high losses. In [3], transition matrix is used to design a novel lowpass–bandpass diplexer with a small size. The design becomes more difficult when the distance between the cut-off frequency of the first band (f_c) and the resonant frequency of the second band (f_r) decreases. The distances between the lowpass and bandpass channels of the proposed diplexers presented in [1–4] are large, which make these designs easier. However, the losses in [4] are high. Although the ratio of f_r/f_c is decreased in [5], it has two disadvantages: large size and high losses. In [6, 7], the frequency ratio (f_r/f_c) is also high. The designed diplexer in [7] is very small, but it has a narrow bandpass channel with a very low fractional bandwidth (FBW). The oldest lowpass–bandpass diplexer is presented in [8]. It has several disadvantages in terms of large implementation area, lack of sharp edge of the lowpass channel, large losses, and narrow bandpass channel. The other important parameter in the diplexer design is the flatness of passbands. Having a low group delay ensures the flatness of passbands. Despite the importance of group delay, many diplexer designers have not addressed this issue. In [3], [5], and [6], the group delays are calculated where all of them have high group delays at their lowpass channels. The microstrip bandpass–bandpass diplexers in [9–11] have high group delays at both channels.

This paper presents a compact microstrip lowpass–bandpass diplexer with low losses, which is suitable for modern wireless communication systems. Compared with the previous designs, the distance between the lowpass channel cut-off frequency and the bandpass resonance frequency is shorter, making the proposed diplexer more challenging to design. However, in this work, we will try to keep our diplexer small in size with good performance. First, a lowpass microstrip resonator will be proposed and discussed to design our diplexer. Then it will be upgraded to a lowpass filter (LPF). Next, the dimensions of important parts of this filter will be optimized to achieve the best frequency response. After that, an optimized bandpass resonator will be added to our LPF to complete the diplexer layout. Our design method is based on a mathematical analysis to extract some information about the important microstrip cells. Based on this information, the optimization is done to miniaturize the overall size. Finally, a perfect comparison between our and previous works will be made to show the advantages of this work.

Designing method

The topology of the proposed diplexer is presented in Fig. 1. It consists of the integrated LPF and BPF. The lowpass section includes three shunt stubs loaded on a transmission line. The shunt stubs admittances are Y_a and Y_b. The physical and electrical lengths of each part of the transmission line are shown with l and θ, respectively. The BPF is composed of a spiral cell connected to a pair of coupled lines. As shown in Fig. 1, the coupling between two lines can create several capacitors. A passband channel will be created when these capacitors connect to the spiral cell because the spiral cell has an inductance feature. The order of the filters should be selected to achieve a minimum size while we have a relatively high degree of freedom in the design. Hence, the shunt stubs for the LPF seems like a suitable choice. The order of the BPF can be selected according to the LPF size. Because as shown in Fig. 1, these filters should occupy the minimum area together.

Design and analysis of the proposed LPF

To analyze the LPF, we can calculate its transmission matrix (T). Then, by using it the conditions of loss reduction and transmission zeros can be determined. The transmission matrix of the lowpass section in Fig. 1 is obtained as follows:

$$T = \begin{bmatrix} A & B \\ C & D \end{bmatrix} = \begin{bmatrix} 1 & 0 \\ Y_a & 1 \end{bmatrix} \times \begin{bmatrix} \cos\theta & jz\sin\theta \\ \dfrac{j\sin\theta}{z} & \cos\theta \end{bmatrix} \times \begin{bmatrix} 1 & 0 \\ Y_b & 1 \end{bmatrix} \times \begin{bmatrix} \cos\theta & jz\sin\theta \\ \dfrac{j\sin\theta}{z} & \cos\theta \end{bmatrix} \times \begin{bmatrix} 1 & 0 \\ Y_a & 1 \end{bmatrix} \rightarrow$$

where:

$$\begin{aligned} A =& \cos^2\theta + jzY_b\cos\theta\sin\theta - \sin^2\theta \\ &+ Y_a(2jz\cos\theta\sin\theta - z^2Y_b\sin^2\theta\cos\theta) \\ B =& 2jz\cos\theta\sin\theta - z^2Y_b\sin^2\theta\cos\theta \\ C =& (Y_b + Y_a)\cos^2\theta + \cos\theta\sin\theta \\ &\left(\frac{2}{z}j + jzY_aY_b\cos\theta - Y_a\sin\theta\right) + Y_aD \\ D =& Y_ajz\sin\theta\cos\theta - \sin^2\theta\,(1 + z^2Y_aY_b\cos^2\theta) \\ &+ \cos^2\theta\,(jz(Y_b + Y_a)\sin\theta + 1) \end{aligned} \quad (1)$$

and

$$\theta = \frac{\omega_c\sqrt{\varepsilon_{re}}}{300}l$$

where θ, l, ω_c, and ε_{re} are the electrical length, physical length (presented in Fig. 1), angular cut-off frequency of the LPF, and effective dielectric constant, respectively. The perfect impedance matching leads to decrease the return loss significantly. In equation (1), the matrices containing the terms of $\sin\theta$ and $\cos\theta$ are related to the transmission lines with the electrical length θ in Fig. 1 (lowpass part). The other matrices are related to the shunt stubs of the LPF. A high impedance matching is one of the factors which can help to decrease the return loss. To achieve this advantage, the reflection coefficient should be near zero. The reflection coefficient of the lowpass cell (Γ) is calculated as follows:

$$\Gamma = \frac{A + B - C - D}{A + B + C + D} \quad (2)$$

For perfect matching: $\Gamma = 0$. Therefore, $A + B = C + D$ and as a result:

$$\begin{aligned} jz\left(Y_b + Y_a + 2 - Y_a^2 - \frac{2}{z^2}\right) =& z[Y_b + 2Y_a]\cot\theta \\ &- Y_a\tan\theta + jz(Y_b + Y_a + 2Y_aY_b + Y_a^2)\cos\theta \\ &+ (Y_aY_bz^2 + Y_bz^2 + Y_a)\sin\theta \\ &- z^2Y_aY_b(1 + Y_a)\sin\theta\cos\theta \end{aligned} \quad (3a)$$

Due to the symmetrical structure of the LPF network, the reflection coefficient in the output port of the LPF is exactly the same as its input port. For predetermined values of cut-off frequency, ε_{re} and l, the above equation will be in terms of admittances. This means that from equation (3), for the predetermined values of cut-off frequency, dielectric constant, and the electrical length θ, we can adjust the values of shunt

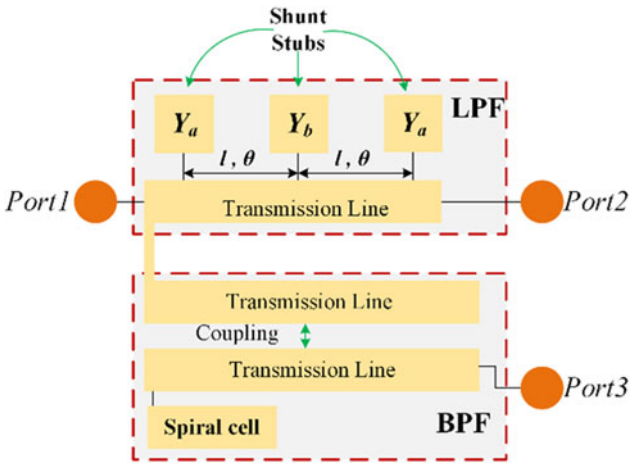

Fig. 1. Basic structure of the proposed diplexer.

https://doi.org/10.1017/S1759078722001465 Published online by Cambridge University Press

stubs. If the shunt cells are low-impedance, then we can write the following equation and replace it in equation (3a) as follows:

$$\begin{cases} Y_b + Y_a + 2 - \dfrac{2}{z^2}\langle\langle Y_a^2 \\ Y_b + Y_a\langle\langle 2Y_aY_b + Y_a^2 \\ Y_aY_bz^2\rangle\rangle Y_bz^2 + Y_a \end{cases} \rightarrow$$

$$zY_a^2 = -j[z[Y_b + 2Y_a]\cot\theta - Y_a\tan\theta + jz(2Y_aY_b + Y_a^2)\cos\theta + (Y_aY_bz^2)\sin\theta - z^2Y_aY_b(1 + Y_a)\sin\theta\cos\theta] \quad (3b)$$

For predetermined values of $l = 6.5$ mm, $\varepsilon_{re} = 1.72$ and 1.67 GHz cut-off frequency, we calculated $\theta = 17°$. Then, we can simplify equation (3b) as follows:

$$zY_a^2 = -j[z3.2[Y_b + 2Y_a] - 0.3Y_a + 0.95jz(2Y_aY_b + Y_a^2) + 0.29(Y_aY_bz^2) - 0.27z^2Y_aY_b(1 + Y_a)] \quad (3c)$$

From the above equation, we can obtain the ratio of shunt rectangular admittances which help us to easier optimization. The characteristic impedance z will be found based on the length and width of the transmission line as well as the dielectric layer thickness [16]. Equation (3) can be generalized for lowpass prototype filters with ladder equivalent circuit.

As presented in Fig. 1, our proposed LPF consists of three shunt stubs loaded on a simple transmission line. We have assumed that the two side stubs are similar and different from the middle stub. The transmission line with the physical length $2l$ at the low frequency will be short-circuited. Therefore, a short circuit path will be created between the input and output ports. Hence, it resonates at the low frequencies. The shunt stubs can be the cells filled with copper, which can be used to control the sharpness, harmonics S_{11}, and insertion loss. Another choice of shunt stubs can be the step impedance cells. The *LC* model of step impedance cell includes capacitors and inductors. We can upgrade this basic structure to an LPF. The optimization method can be very helpful in improving the filter performance.

The layout of our LPF is presented in Fig. 2(a). We have placed all the stubs at the top of the transmission line so that there is enough space at the bottom to accommodate the bandpass resonator. This makes the size more compact. A large negative value of S_{11} in the passband is a transition pole. As shown in Fig. 2, a T-shape step impedance cell is embedded in the middle which can control the harmonics and create a transition pole, simultaneously. To increase the degree of freedom in controlling the frequency response, four rectangular cells are used. Instead of a rectangular resonator, any low-impedance resonators such as radial or triangular types can be utilized. In general, the space created by copper for moving the current is important. However, using the rectangular resonators helps to reduce the overall size. Therefore, we used the rectangular resonators instead of the other types of resonators. The overall dimensions of this resonator are obtained by the optimization method. Moreover, two tapped line feed structures are utilized to decrease the losses at the passband. The overall size of the designed LPF is $0.24\,\lambda_g \times 0.099\,\lambda_g$ (33.9 mm × 14.1 mm), where λ_g is the guided wavelength calculated at the cut-off frequency of the lowpass channel. Hence, the normalized circuit size of this LPF is NCS = 0.023 (λ_g^2/mm^2). The important physical dimensions in optimizing the frequency response are l_a, l_b, l_c, l_d, w_a, and w_b. The frequency response of the proposed LPF is shown in Fig. 2(b). The cut-off frequency and −20 dB stopband frequency of

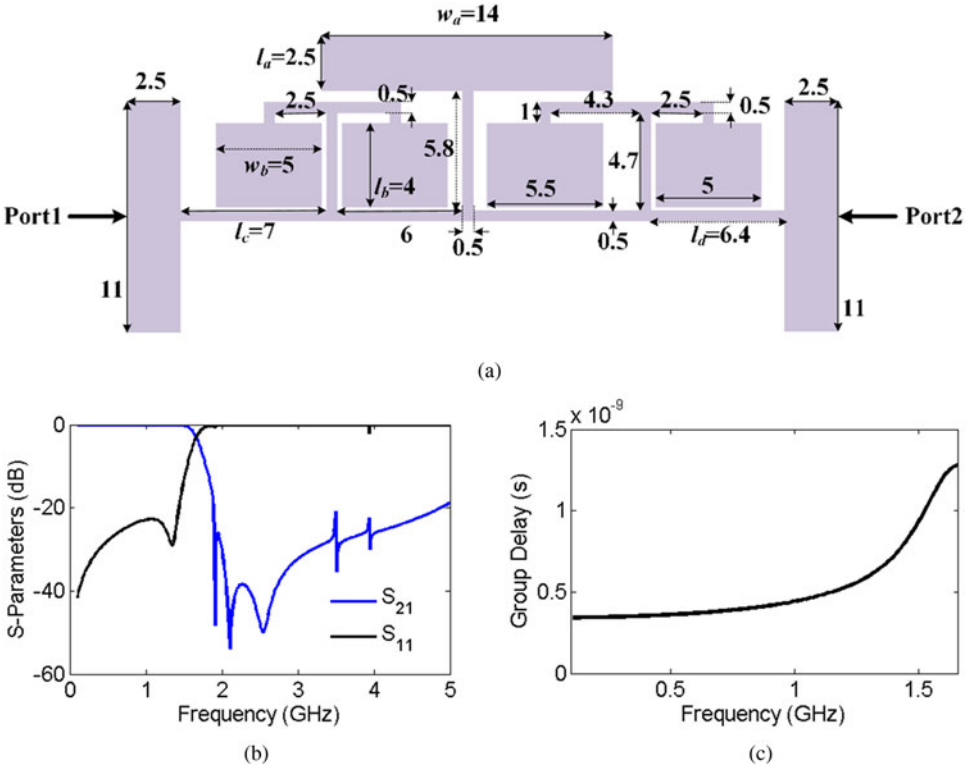

Fig. 2. Proposed LPF: (a) layout (unit: mm), (b) simulated S_{21} and S_{11}, (c) group delay.

https://doi.org/10.1017/S1759078722001465 Published online by Cambridge University Press

our LPF are $f_c = 1.67$ GHz and $f_s = 1.88$ GHz, respectively. It has an insertion loss (IL) of 0.047 dB and an S_{11} of −22.7 dB. The sharpness factor is $\xi = 80.95$ (dB/GHz), where$\xi = 17/(f_s - f_c)$. The harmonics are attenuated up to 4.88 GHz with a maximum harmonic level of −20 dB. Therefore, it has a relative stopband bandwidth of RSB = Stop band Band width/$fc = 1.93$ with a suppression factor of SF = Maximum Harmonic Level/10 = 2. Our proposed LPF has a two-dimensional structure. Hence, it has an architecture factor of AF = 1. To compare with the other LPFs, having a high Figure Of Merit (FOM) is a good option where FOM = $(\xi \times SF \times RSB)/(NCS \times AF)$. The FOM of this LPF is 13585.52 which is good in comparison with the previous works. Another factor to compare LPFs is OFOM = FOM × RL/IL, where IL is the insertion loss. OFOM of our LPF is 6561517.94 which is a very good value. Another advantage of this LPF is its flat channel with a low group delay of 1.27 ns, where Fig. 2(c) depicts the group delay of our LPF. This LPF is simulated by ADS software (EM simulator) on an RT/Duroid 5880 substrate with $\varepsilon_r = 2.22$, $h = 0.7874$ mm, and tan $(\delta) = 0.0009$. In this work, all simulation results are obtained on the above substrate using ADS software.

The dimensions of the designed LPF are optimized. The effects of changing physical dimensions on the frequency response are shown in Figs 3(a)–3(f). Changing the physical length l_a directly affects the harmonics. This is presented in Fig. 3(a), where decreasing l_a increases the harmonic level. On the other hand, by choosing an average value of this length we can create two transition poles at the passband. Another physical length that effects on harmonic level is l_b, which is depicted in Fig. 3(b). As shown in Fig. 3(b), having longer l_b leads to suppress the harmonics and better return loss (RL). Figures 3(c) and 3(d) show that by tuning l_c and l_d we can achieve lower RL. The simulation results show that wherever the RL is better, the IL is reduced. Figure 3(e) shows that the shunt stub with the physical width w_a has an important effect on the harmonic level, so that reducing w_a products some undesired harmonics. As shown in Fig. 3(f), by adjusting w_b, a transmission pole can be generated.

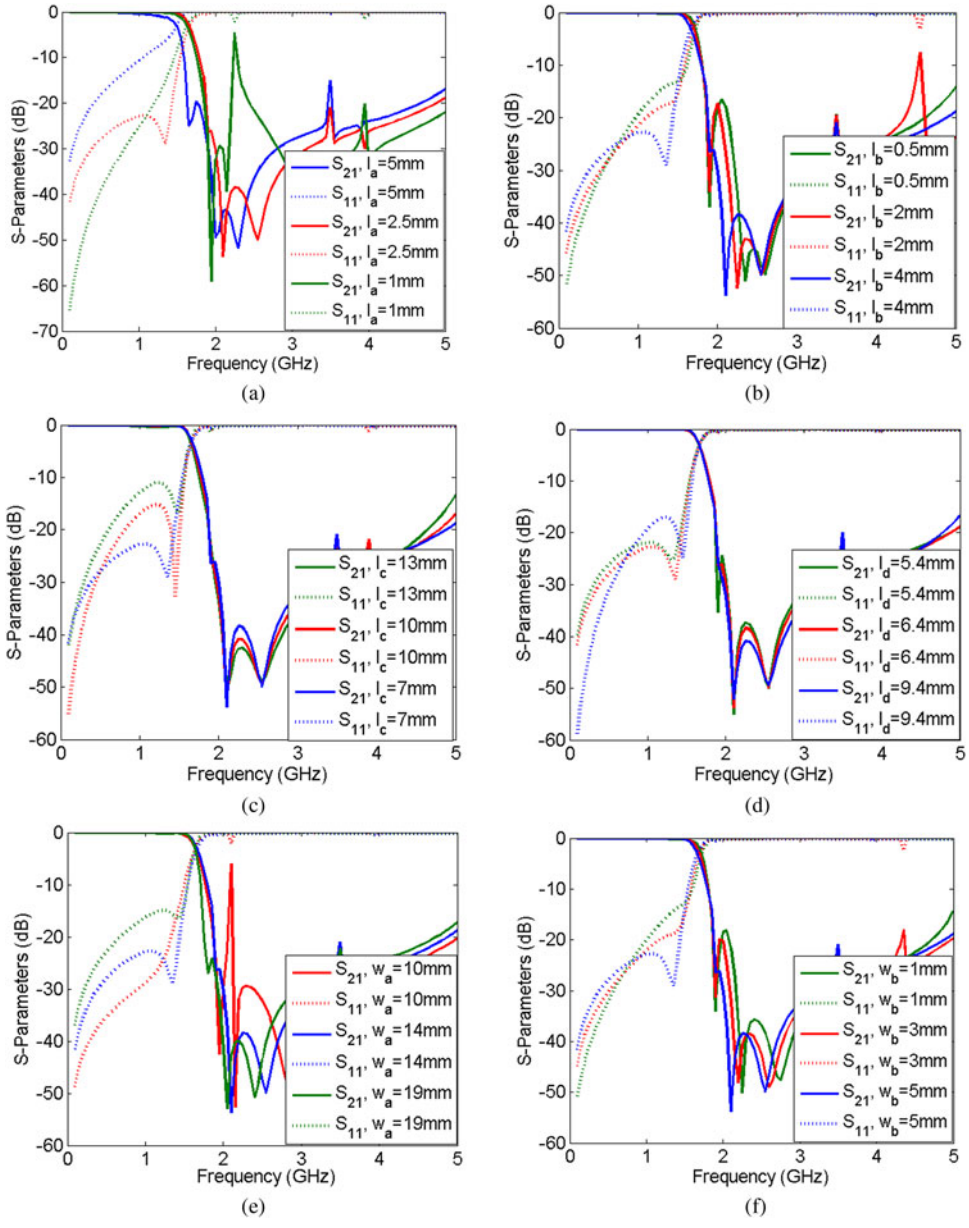

Fig. 3. Frequency response of the proposed LPF as functions of: (a) l_a, (b) l_b, (c) l_c, (d) l_d, (e) w_a, (f) w_b.

https://doi.org/10.1017/S1759078722001465 Published online by Cambridge University Press

Design and analysis of the proposed BPF

The basic structure of our BPF is indicated in Fig. 4. The coupling effect is presented with three coupled capacitors of C_1 which is an approximated model of coupled lines. Each transmission line is divided into two equal lines with the physical length l_1, electrical length θ_1, and characteristic impedance Z_1. Also, we assume that the electrical length and characteristic impedance of spiral cell are θ_2 and Z_2 respectively.

The input admittance of this filter can be calculated as follows:

$$Y_{in}=\cfrac{1}{\cfrac{1}{\cfrac{1}{\cfrac{1}{\cfrac{1}{2jZ_1\tan(\theta_1)+\cfrac{1}{j\omega C_1}}+j\omega C_1}+2jZ_1\tan(\theta_1)}+j\omega C_1}+jZ_2\tan(\theta_2)} \tag{4}$$

In equation (4), Z_1 and Z_2 are the characteristic impedances of the transmission line with the physical length l_1 and the spiral cell, respectively. To obtain resonance frequencies, Y_{in} must be zero. Therefore, the angular resonance frequencies ω_1 and ω_2 can be calculated as shown in equation (5).

$$3-8\omega C_1Z_1\tan(\theta_1)+4\omega^2C_1^2Z_1^2\tan^2(\theta_1)=0$$
$$\Rightarrow\begin{cases}\omega_2=\dfrac{8C_1Z_1\tan(\theta_1)-\sqrt{48C_1^2Z_1^2\tan^2(\theta_1)}}{8C_1^2Z_1^2\tan^2(\theta_1)}=\dfrac{0.1}{C_1Z_1\tan(\theta_1)}\\ \omega_1=\dfrac{8C_1Z_1\tan(\theta_1)+\sqrt{48C_1^2Z_1^2\tan^2(\theta_1)}}{8C_1^2Z_1^2\tan^2(\theta_1)}=\dfrac{1.8}{C_1Z_1\tan(\theta_1)}\end{cases} \tag{5}$$

Since we need a single-mode resonator, one of the angular resonance frequencies is a harmonic which should be attenuated or completely removed. From equation (5), if $\tan(\theta_1)$ is a large number, then the values of ω_1 and ω_2 will be close to each other. However, this method leads to a significant increasing of l_1. Another way to get rid of this harmonic is to set it at a very high frequency. The characteristic impedance of Z_1 can be obtained as follows [16]:

$$Z_1=\frac{60}{\sqrt{\varepsilon_{re}}}\ln\left(8\frac{h}{w_1}+0.25\frac{w_1}{h}\right)\text{ and }\frac{w}{h}\le 1$$
where:
$$\varepsilon_{re}=\frac{\varepsilon_r+1}{2}+\frac{\varepsilon_r-1}{2}\left[\frac{1}{\sqrt{1+12\frac{h}{w_1}}}+0.04\left(1-\frac{w_1}{h}\right)^2\right] \tag{6}$$

Where ε_r, ε_{re}, h, and w_1 are the dielectric constant, effective dielectric constant, thickness of dielectric, and the width of transmission line with physical length l_1, respectively. If $w_1 = 0.3$ mm, $h = 0.7874$ mm, and $\varepsilon_r = 2.22$, then from equation (6) $\varepsilon_{re} = 1.72$ and $Z_1 = 144.2\,\Omega$. At a predetermined target resonance frequency of $f_{r1} = 2.6$ GHz, the value of θ_1 is $(4.1l_1)°$ which is calculated from equation (1). By replacing these values in equation (5), the following equation can be obtained:

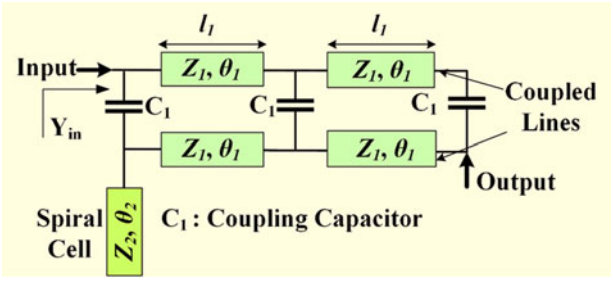

Fig. 4. Basic structure of the proposed BPF.

$$\omega_1=2\pi f_{r1}=\frac{0.1}{144.2C_1\tan(4.1l_1)}\Rightarrow C_1\tan(4.1l_1)\approx 4.24\times10^{-14} \tag{7}$$

If $l_1 = 10.3$ mm, then C_1 will be 0.046 pF which is an acceptable value when the space between coupling lines is a little increased. Because C_1 is a coupling capacitor that is usually a small value in pF, by increasing the space between coupled lines, the value of C_1 is decreased. For $l_1 = 10.3$ mm, the second angular resonance frequency can be obtained as follows:

$$\omega_2=2\pi f_{r2}=\frac{1.8}{144.2\times4.6\times10^{-14}\times\tan(42.23)}\Rightarrow f_{r2}\approx 47.5\,\text{GHz}\Rightarrow f_{r2}\rangle\rangle f_{r1} \tag{8}$$

Therefore, by placing the second resonance frequency at a far distance from the first one, we get rid of this harmonic. In the proposed BPF structure, $l_1 = 10.3$ mm with 0.3 mm width so that the overall size of coupled lines is 20.6 mm. The proposed bandpass structure is carefully designed and directly connected to the LPF filter without any extra matching circuits. This leads to have a high-performance microstrip diplexer with good passband characteristics. To find the ABCD matrix and reflection coefficient of the BPF (T_B and Γ_B) we assumed that the impedances of the coupled lines and spiral cells are Z_C and Z_S, respectively. Similar to the analysis of the LPF, T_B, Γ_B, and the condition for perfect matching ($\Gamma_B = 0$) can be obtained as follows:

$$T_B=\begin{bmatrix}1 & Z_C\\ 0 & 1\end{bmatrix}\times\begin{bmatrix}1 & 0\\ \frac{1}{Z_S} & 1\end{bmatrix}=\begin{bmatrix}1+\frac{Z_C}{Z_S} & Z_C\\ \frac{1}{Z_S} & 1\end{bmatrix}\rightarrow$$
$$\Gamma_B=\frac{\frac{Z_C}{Z_S}+Z_C-\frac{1}{Z_S}}{2+\frac{Z_C}{Z_S}+Z_C+\frac{1}{Z_S}} \tag{9}$$
$$\Gamma_B=0\rightarrow Z_C=\frac{1}{1+Z_S}$$

From equation (9), if $Z_C = 1/(1 + Z_S)$ then we have a perfect matching in the output port of the BPF.

The proposed diplexer (structure and simulation results)

Usually, the design of lowpass–bandpass diplexers is started with the design of LPF and BPF separately, and then they are

https://doi.org/10.1017/S1759078722001465 Published online by Cambridge University Press

connected to each other using an extra matching circuit. However, we connected the proposed LPF to the analyzed BPF directly without an extra matching network. This method leads to save the size diplexer. Since the coupled lines are important parts of bandpass resonators, we used them in our diplexer design. Actually, the required capacitors to form the passband are supplied through the coupled lines. Spiral cells are our other choice for connecting to coupled lines, because they are inductors that are easily adjustable and at the same time take up less space. Accordingly, our proposed diplexer is depicted in Fig. 5(a). As can be seen, we set the lengths and widths of coupled lines equal to 20.6 and 0.3 mm respectively. These values are obtained from the analyzed BPF in the previous section.

As mentioned above, the bandpass section consists of a pair of coupled lines connected to spiral transmission lines. The advantage of this structure is the direct connection without using machining circuits. We also do not have to change the LPF structure to eliminate the loading effect. The overall size of our lowpass–bandpass diplexer is 0.15 $\lambda_g \times 0.24\ \lambda_g$ (21.3 mm × 33.9 mm), where λ_g is the guided wavelength calculated at the cut-off frequency of the lowpass channel. The more important physical dimensions in the optimization process are l_e, l_f, l_g, l_h, and the space between coupled lines (S). We fixed them on the best values to get the best frequency response. The frequency response of our designed diplexer is shown in Figs 5(b) and 5(c). As it can be seen, the bandpass channel is from 2.39 to 2.76 GHz, where it resonates at $f_r = 2.57$ GHz with a fractional bandwidth of FBW = 14% and an insertion loss of $IL_B = 0.16$ dB. The cut-off frequency of the lowpass channel is not changed significantly. It is located at $f_c = 1.65$ GHz with a low insertion loss of $IL_L = 0.047$ dB. The S_{11} at the lower and upper passbands are better than −21.8 and −20.9 dB, respectively, where there is a −30 dB transmission pole at the lowpass channel. As illustrated in Fig. 5(c), the simulated isolation between ports 2 and 3 is better than −21.2 dB. The harmonics are suppressed up to 4.3 GHz (2.6 f_c), where there is a maximum harmonic level of −20 dB. A harmonic is defined as a positive integer multiple of cut-off frequency of the lowpass channel.

To show how we adjusted the important physical dimensions, we present their effects on the frequency response in Figs 6(a)–6(e). As shown in these figures, changing these parameters does not have a significant effect on the lower passband. Figure 6(a) shows that the choice of a low value of l_e is more appropriate, because harmonics appear with the increase of it. Although an increase in l_f pushes the resonance frequency to the left, but it can create undesired harmonics after the passband. However, as shown in Fig. 6(b) for suppressing the harmonics below and above the passband we have to select a middle value of l_f. Figure 6(c) depicts that increasing l_g can move the resonance frequency to the left. As illustrated in Fig. 6(d), as the length l_h increases the passband becomes narrower. On the other hand, with increasing this length the level of harmonics will be decreased. Figure 6(e) shows that increasing and decreasing the distance between the coupling lines will lead to the failure of the passband so we had to choose a middle value for this distance. Another important factor in determining the performance of a diplexer is the group delay, which is not mentioned in most of the previous

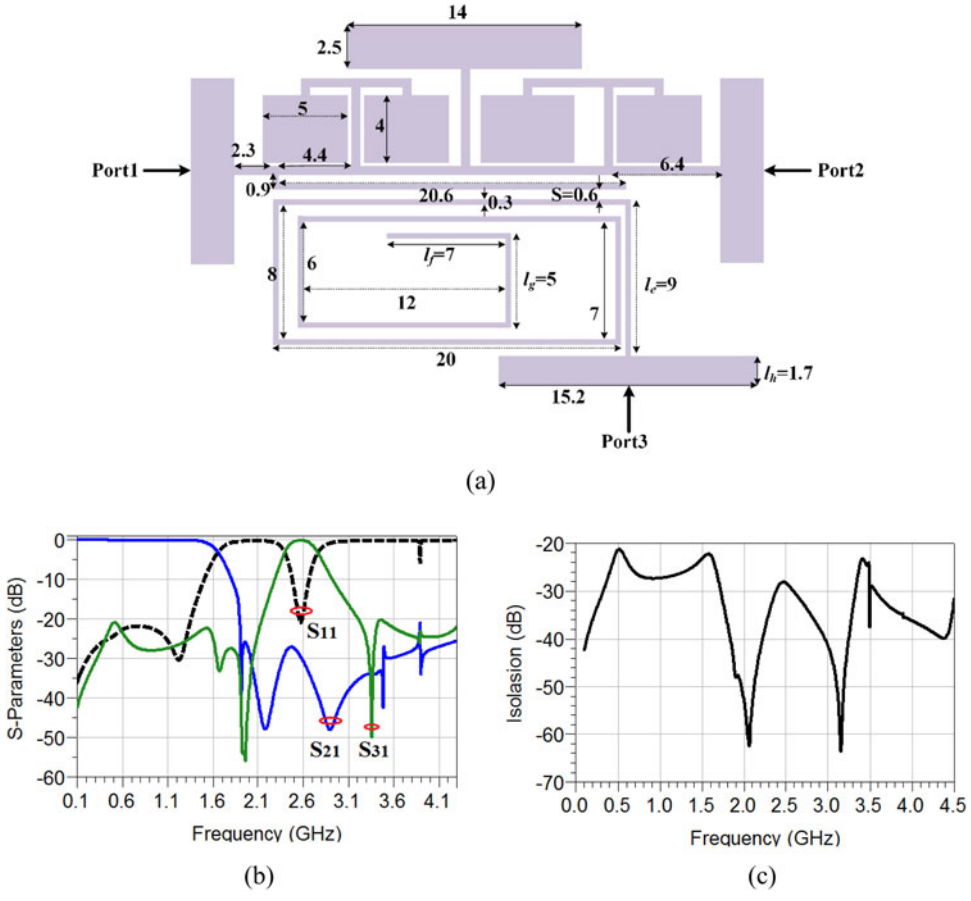

Fig. 5. Proposed diplexer (a) layout (unit: mm), (b) transition parameters and S_{11}, (c) isolation between channels.

https://doi.org/10.1017/S1759078722001465 Published online by Cambridge University Press

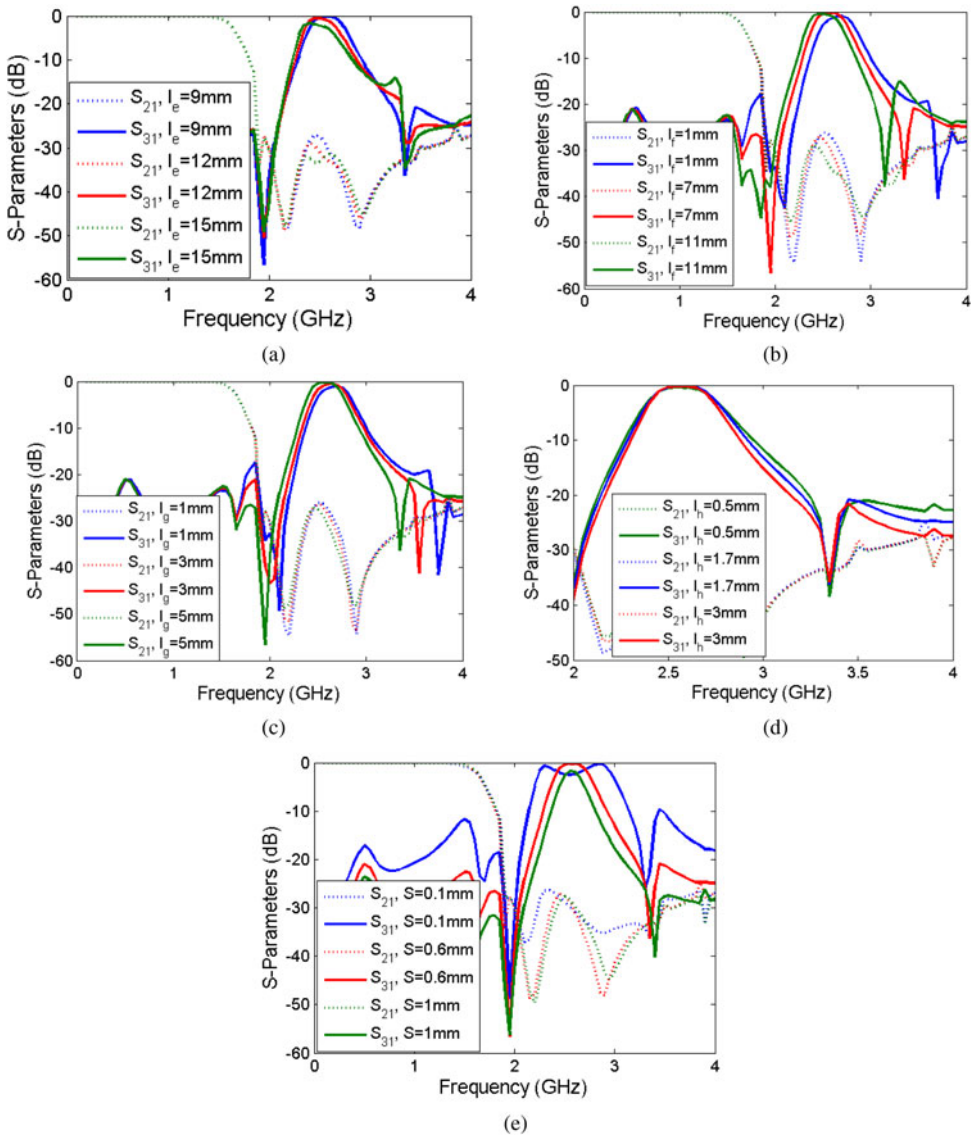

Fig. 6. Frequency response of the proposed diplexer as functions of (a) l_e, (b) l_f, (c) l_g, (d) l_h, (e) S.

diplexers. Having a flat passband channel is an advantage that depends on low group delay. Therefore, group delay is more significant within the bandwidth. The group delay is very low at both channels of our diplexer. It is lower than 1.68 and 1.4 ns at the lowpass and bandpass channels, respectively. The maximum group delays at the lower and upper channels occur at 1.65 and 2.44 GHz, respectively. Figures 7(a) and 7(b) show the group delays of S_{21} and S_{31} within the lowpass and bandpass channels.

Results and comparison

The proposed diplexer is fabricated and measured and there is a good agreement between simulation and measurement results. An N5230A network analyzer is used to measure the fabricated diplexer. In Fig. 8(a) the comparison between the simulation and measurement results for *S*-parameters of the proposed diplexer is shown. Also, Fig. 8(b) shows the fabricated diplexer.

To show the features of this work, our proposed diplexer is compared with the previously reported diplexers as shown in Table 1. The comparison results consist of size, losses, FBW, and the frequency ratio f_r/f_c. It is clear that our diplexer occupies a compact area while it has good FBW, low frequency ratio, low IL, and good common port RL at both channels. The simulation results show that obtaining a diplexer when its channels are close together is more difficult. Usually, having close channels in a diplexer is inversely related to improving its isolation, selectivity, and losses. On the other hand, close channels make diplexer suitable for FDD schemes [17]. Hence, having a high-performance diplexer with close channels is an important advantage. Although the proposed diplexer in [5] could design a diplexer with lower frequency ratio than ours, it has very large size and higher ILs at both channels. We were able to reduce the losses better than others, because the maximum IL and S_{11} of our diplexer are 0.16 and −20.9 dB, respectively, which are better than other previous designs.

As it can be seen in Table 1, only the presented diplexers in [3] and [7] have smaller sizes than ours. However, both of them have high frequency ratios, while in [7] the bandpass channel is narrow. Some designers obtained negative group delays out of −3 dB passband frequencies [12, 13]. A negative group delay does not break causality [13]. However, at the first resonance frequency

https://doi.org/10.1017/S1759078722001465 Published online by Cambridge University Press

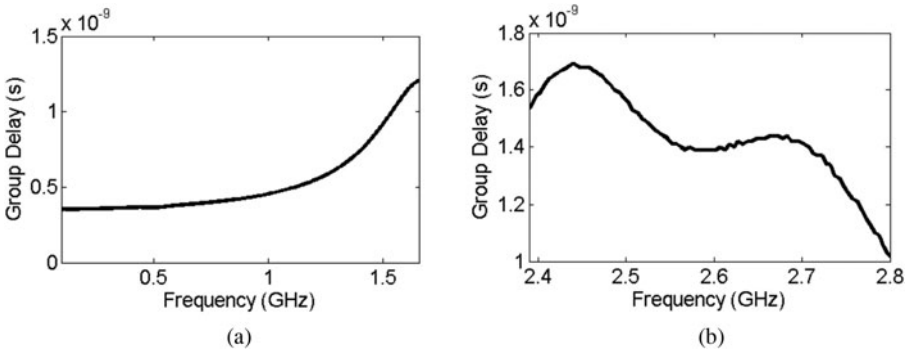

Fig. 7. Group delay within (a) the lowpass channel, (b) the bandpass channel.

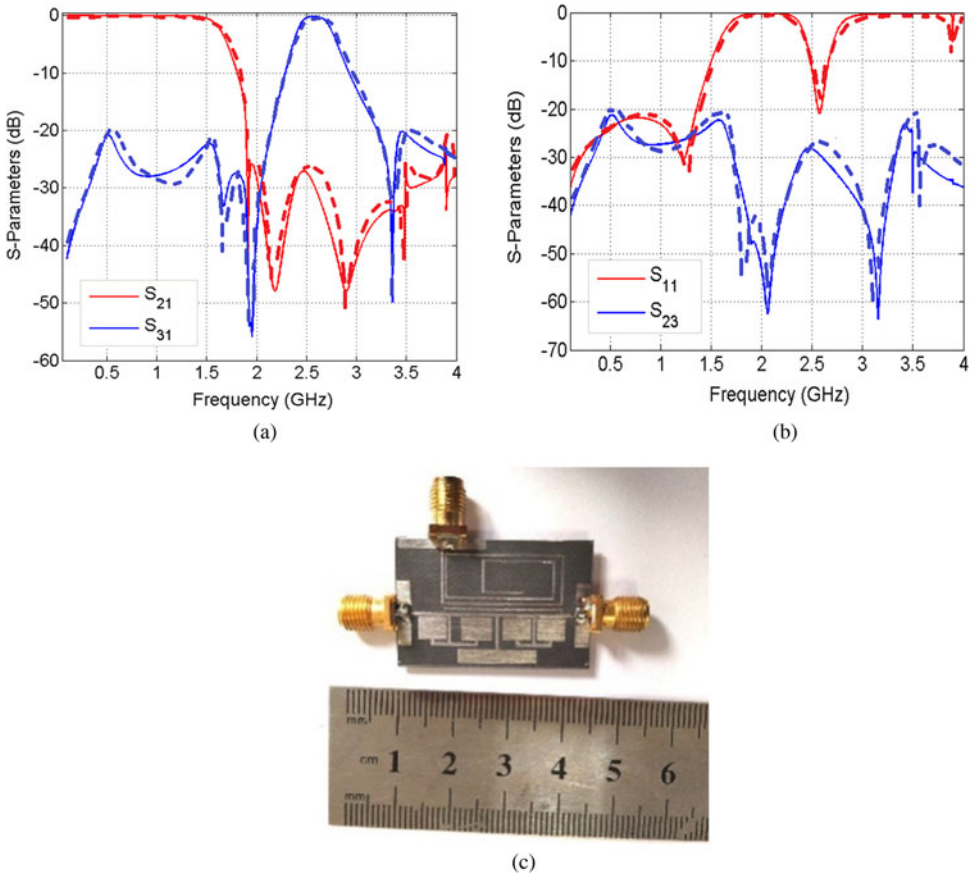

Fig. 8. (a) Comparison between the simulation (solid lines) and measurement (dashed lines) results, (b) fabricated diplexer.

Table 1. Comparison between the lowpass–bandpass diplexers

References	f_c, f_r (GHz)	IL_L, IL_B (dB)	S_{11} (dB)	FBW%	Size (λ_g^2)	f_r/f_c
This work	1.65, 2.57	0.047, 0.16	−21.8, −20.9	14	0.037	1.5
[1]	2, 3.5	0.3, 1.28	Better than −15	5	0.095	1.75
[2]	1.5, 2.4	0.25, 2.42	–	8	–	1.6
[3]	1.88,3.56	0.12, 0.10	−19.2, −36	23	0.03	1.9
[4]	1, 2.4	0.25, 0.58	−15, −30	–	0.046	2.4
[5]	2.64, 3.73	0.2, 0.25	−18, −15.58	18	0.075	1.41
[6]	2.4, 4.2	0.15, 0.18	−18.2, −41.4	15.2	0.036	1.75
[7]	1.57, 3.35	0.01, 0.26	−31, −16	4.7	0.018	2.1
[8]	1.5, 2.4	0.25, 2.42	−15, −15	7.6	0.49	1.6

https://doi.org/10.1017/S1759078722001465 Published online by Cambridge University Press

Table 2. Maximum group delay (MGD) comparison

References	MGD at the first channel (ns)	MGD at the second channel (ns)	Diplexer type
This work	1.43	1.68	Lowpass–bandpass
[3]	2	1.24	Lowpass–bandpass
[5]	2.25	2.75	Lowpass–bandpass
[6]	2.8	1.36	Lowpass–bandpass
[9]	3.15	2.98	Bandpass–bandpass
[10]	3	3.14	Bandpass–bandpass
[11]	2.2	2.6	Bandpass–bandpass

of the presented diplexer in [13] we can see a very high group delay of 46.1 ns. The group delay of this work is compared with previous lowpass–bandpass and bandpass–bandpass diplexers. It should be noted that other references did not mention group delay information. As presented in Table 2, the minimum group delay at the first channel is obtained in our diplexer, while the group delay at the second channel is acceptable.

Conclusion

In this work, a small microstrip lowpass–bandpass diplexer with good performance is provided. The cut-off and resonance frequencies of the proposed diplexer make it suitable for modern wireless communication systems. Due to low losses, it is appropriate for energy harvesting applications. Another feature of our diplexer is its flat channels with low group delays. Its lowpass channel has a sharp roll-off with a high figure of merit and OFOM. The introduced diplexer could suppress the first and second harmonics with a maximum harmonic level of −20 dB. Due to the lack of needing an extra matching circuit, the size of the proposed diplexer has been significantly reduced.

Acknowledgements. The authors would like to acknowledge the financial support of Kermanshah University of Technology for this research under grant number S/P/T/1439.

Conflict of interest. None.

References

1. **Elden S and Gorur AK** (2021) Design of a compact lowpass-bandpass diplexer with high isolation. *Progress in Electromagnetics Research Letters* **97**, 21–26.
2. **Deng P-H and Tsai J-T** (2013) Design of microstrip lowpass-bandpass diplexer. *IEEE Microwave and Wireless Components Letters* **23**, 332–334.
3. **Hayati M, Rezaei A and Noori L** (2019) Design of a high-performance lowpass–bandpass diplexer using a novel microstrip structure for GSM and WiMAX applications. *IET Circuits, Devices & Systems* **13**, 361–367.
4. **Heshmati H and Roshani S** (2018) A miniaturized lowpass bandpass diplexer with high isolation. *AEU – International Journal of Electronics and Communications* **87**, 87–94.
5. **Nouri L, Yahya S and Rezaei A** (2020) Design and fabrication of a low-loss microstrip lowpass-bandpass diplexer for WiMAX applications. *China Communications* **17**, 109–120.
6. **Rezaei A, Noori L and Jamaluddin MH** (2019) Novel microstrip lowpass-bandpass diplexer with low loss and compact size for wireless applications. *AEU-International Journal of Electronics and Communications* **101**, 152–159.
7. **Yahya SI, Rezaei A and Nouri L** (2020) A novel miniaturized microstrip lowpass bandpass diplexer using patch and interdigital cells for wireless networks. *AEU-International Journal of Electronics and Communications* **126**, 1434–8411.
8. **Capstick M-H** (1999) Microstrip lowpass-bandpass diplexer topology. *Electronics Letters* **35**, 1958–1960.
9. **Noori L and Rezaei A** (2017) Design of a microstrip diplexer with a novel structure for WiMAX and wireless applications. *AEU-International Journal of Electronics and Communications* **77**, 18–22.
10. **Rezaei A and Noori L** (2018) Compact low-loss microstrip diplexer using novel engraved semi patch cells for GSM and WLAN applications. *AEU-International Journal of Electronics and Communication* **87**, 158–163.
11. **Rezaei A, Yahya SI, Noori L and Jamaluddin MH** (2019) Design of a novel wideband microstrip diplexer using artificial neural network. *Analog Integrated Circuits and Signal Processing* **101**, 57–66.
12. **Majdi KA and Mezaal YS** (2022) Microstrip diplexer for recent wireless communities. *Periodicals of Engineering and Natural Sciences* **10**, 387–396.
13. **Hussein HA, Mezaal YS and Alameri BM** (2021) Miniaturized microstrip diplexer based on FR4 substrate for wireless communications. *Elektronika Ir Elektrotechnika* **27**, 34–40.
14. **Yahya SI, Rezaei A and Nouri L** (2021) The use of artificial neural network to design and fabricate one of the most compact microstrip diplexers for broadband L-band and S-band wireless applications. *Wireless Networks* **27**, 663–676.
15. **Yahya SI, Rezaei A and Yahya RI** (2022) A new ANFIS-based hybrid method in the design and fabrication of a high-performance novel microstrip diplexer for wireless applications. *Journal of Circuits, Systems and Computers* **31**, 2250050.
16. **Hong JS and Lancaster MJ** (2001) *Microstrip Filters for RF/Microwave Applications*. Hoboken, New Jersey, USA: John Wiley & Sons.
17. **Rezaei A, Noori L and Mohammadi H** (2017) Design of a novel compact microstrip diplexer with low insertion loss. *Microwave and Optical Technology Letters* **59**, 1672–1676.

Abbas Rezaei is an associate professor of electrical engineering in Kermanshah University of Technology. He obtained B.Se., M.Se., and Ph.D. in electronics engineering from Razi University, Kermanshah, Iran, in 2005, 2009, and 2013, respectively. His current research interests include RF and microwave circuits and computational intelligence.

Salah I. Yahya is a professor (full), joined the Department of Software Engineering at Koya University in 2010. He obtained B.Sc. in electrical engineering, an M.Sc. in electronics and communication engineering, and a Ph.D. in communication and microwave engineering. He is a consultant engineer and a senior member of the IEEE-USA and AMTA-USA. Professor Yahya has many published research articles in high-quality journals and he presented many conference papers. His current research interests include antenna design, numerical RF dosimetry, MW measurement, and MW components design. Professor Yahya is a regular reviewer of the Electromagnetics Academy, Cambridge, USA, *PIERS Journals* publications, since 2009, *Science and Engineering of Composite Materials* journal, and *International Journal of Applied Electromagnetics and Mechanics*.

L. Nouri obtained B.Sc. and M.Sc. in electronic engineering from Razi University, Kermanshah, Iran in 2005 and 2009, respectively. She obtained Ph.D. in electronic engineering at the Shiraz University of Technology. Her research interests focus on microstrip coupler, microstrip filter, neural networks, and LNAs.

https://doi.org/10.1017/S1759078722001465 Published online by Cambridge University Press